Journal of Materials Chemistry A

PAPER

View Article Online
View Journal | View Issue

Cite this: J. Mater. Chem. A, 2014, 2, 2397

An experimental and computational investigation of the oxygen storage properties of $BaLnFe_2O_{5+\delta}$ and $BaLnCo_2O_{5+\delta}$ (Ln = La, Y) perovskites†‡

Jonathan W. Lekse,*[a] Sittichai Natesakhawat,[ab] Dominic Alfonso[a] and Christopher Matranga[a]

Received 16th August 2013
Accepted 20th December 2013

DOI: 10.1039/c3ta13257a

www.rsc.org/MaterialsA

One interesting class of materials for oxygen storage applications are double perovskite oxides due to their ability to rapidly store and release oxygen. Previously, the double perovskite $BaYMn_2O_{5+\delta}$ was shown to rapidly and reversibly store and release oxygen with unprecedented kinetics. In this work, four double perovskite materials, $BaLaFe_2O_{5+\delta}$, $BaLaCo_2O_{5+\delta}$, $BaYCo_2O_{5+\delta}$, and $BaYFe_2O_{5+\delta}$, were synthesized and characterized. TGA experimental results for all four samples demonstrate rapid and reversible oxygen storage. The two Fe-containing compounds are the most stable for multiple adsorption/desorption cycles with both nitrogen/air and hydrogen/air at multiple temperatures and have been demonstrated to oxidize methane.

Introduction

Oxygen storage materials are of interest for various applications including air separations,[1] nonaerobic oxidation,[2] syngas preparation,[3] and chemical looping combustion.[4,5] In all of these applications, a material that can store and release oxygen rapidly and reversibly with little or no structural degradation is desirable. Due to their remarkable oxygen storage/release capabilities, perovskite based oxygen carriers provide an interesting alternative to the currently used materials, such as iron and copper oxides.

The perovskite family of materials encompasses a wide variety of metal oxides which are based on the calcium titanium oxide mineral with the general formula ABO_3 discovered in 1839 by Gustav Rose and named for geologist Lev Perovksi. Substitutions can be performed on either the A or B site resulting in double, triple, or even more complex oxide materials. Many of the desirable properties of these materials derive from their ability to be synthesized with both stoichiometric and nonstoichiometric quantities of oxygen. The nonstoichiometric nature of these materials is tied to the presence of cations that can have multiple valence states. The ability of the cations to assume multiple valence states makes these materials interesting for use as superconductors, magnetoresistors, thermoelectric materials, components in solid oxide fuel cells, oxygen storage/separation materials, and oxygen carriers in chemical looping.[6–10]

Another advantage of the nonstoichiometric nature of these materials is they also contain oxygen vacancies, Fig. 1. The presence of vacant oxygen sites means that oxygen transport/diffusion in these materials can occur rapidly. The transport of oxygen coupled with the structural stability of these materials consisting of different quantities of oxygen suggests these compounds have the potential to rapidly take-up and release oxygen, thereby making them ideal for oxygen separation and storage applications processes.

Previous results with double perovskites have demonstrated rapid and reversible uptake and release, in some cases exceeding 2500 μmol g^{-1} at 500 °C.[11–14] Reducing conditions were shown to preferentially remove oxygen atoms from the yttrium plane in $BaYMn_2O_{5+\delta}$ without collapsing the overall

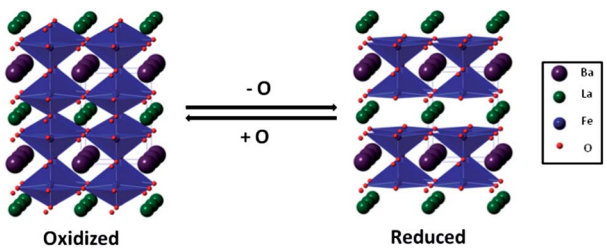

Fig. 1 A schematic representation of the idealized oxidized and reduced double perovskite structures, in which, the oxygen is preferentially lost from channels in the material.

[a]National Energy Technology Laboratory, United States Department of Energy, P. O. Box 10940, Pittsburgh, PA 15236, USA. E-mail: Jonathan.Lekse@CONTR.NETL.DOE.GOV; Tel: +1-412-386-7312

[b]Department of Chemical and Petroleum Engineering, University of Pittsburgh, Pittsburgh, PA 15261, USA

† As part of the National Energy Technology Laboratory's Regional University Alliance (NETL-RUA), a collaborative initiative of the NETL, this technical effort was performed under the RES contract DE-FE0004000.

‡ Electronic supplementary information (ESI) available: Additional powder diffraction patterns and refinement details. See DOI: 10.1039/c3ta13257a

structure.[15,16] Recent computational results have confirmed that the released oxygen atoms originated from the yttrium plane, shedding light on the transport of these atoms through the crystal lattice.[17] Additionally, the stability of perovskite materials has been demonstrated by the cycling of $BaYMn_2O_{5+\delta}$ between O_2 and 5% H_2/95% Ar over 100 times with no discernable change in efficiency.[11] Limited testing of $BaYMn_2O_{5+\delta}$ with CH_4 was also performed where it was observed that combustion began at approximately 450 °C and concluded by 550–600 °C.[11] This previous research with perovskites, which possess a combination of crucial properties (stability, rapid kinetics, *etc.*), and the combined experimental–theoretical efforts detailed herein confirm that this is indeed a promising class of materials.

In this work, four double perovskite compounds, $BaLaFe_2O_{5+\delta}$, $BaLaCo_2O_{5+\delta}$, $BaYCo_2O_{5+\delta}$, and $BaYFe_2O_{5+\delta}$, were targeted for study. Fe and Co were chosen because they are transition metals that possess the capacity for multiple oxidation states necessary to charge balance nonstoichiometric amounts of oxygen in these compounds. La and Y were selected because they are relatively large elements, a characteristic that may facilitate ion transport, and have been used successfully as components in several other oxygen storage materials. The samples in this work were analyzed using a variety of techniques including X-ray diffraction with Rietveld refinement for structural characterization, thermogravimetric analysis for basic oxygen storage studies, and small-scale reactions with methane as a model fuel. Theoretical studies using the VASP code were also conducted in order to understand the fundamental properties that give rise to differences in the oxygen storage capacities of the studied materials.

Experimental methods

Synthesis

Standard powders of (i) $BaCO_3$, Alfa Aesar, 99.95%, (ii) Y_2O_3, Acros Organics, 99.99%, (iii) La_2O_3, Strem, 99.9%, (iv) Fe_2O_3, Aldrich, 99+%, and (v) Co_2O_3, Fisher Scientific, 99.9% were used in this work. Initially, a stoichiometric mixture of starting materials was ground for 15 minutes using a mortar and pestle. The reaction mixture was then placed into an alumina crucible and heated in a muffle furnace in air. The samples were heated from 25 °C to 850 °C at a rate of 1.15° min^{-1}, held at 850 °C for 72 hours, and then cooled from 850 °C to 25 °C at a rate of 1.15° min^{-1}. The resulting material was then ground for 15 minutes and pressed into a pellet which was heated in an alumina crucible in a muffle furnace in air. The temperature profile for this second heating step was a ramp from 25 °C to 1100 °C at a rate of 1.5° min^{-1}, followed by a 120 hour dwell, and finally cooling from 1100 °C to 25 °C at a rate of 1.5° min^{-1}.

Physical property measurements

A PANalytical X'Pert Pro diffractometer was used to collect powder diffraction patterns for the obtained samples. Scans were performed from 5 to 100 degrees 2-theta with a step size of 0.17° and a scan speed of 400 s per degree. Rietveld refinement was performed using Highscore Plus to determine the bulk composition of the samples. Whole pattern refinements using a pseudo-Voigt functional were performed multiple times to achieve the best fit for the collected data.

Thermogravimetric analysis (TGA) was performed on a Mettler Toledo DSC/TGA. A sample of approximately 50 mg was placed into a platinum pan and heated at a rate of 5 °C min^{-1} under flowing air to the desired temperature. The atmosphere in the instrument was then cycled between air and either nitrogen or a mixture of 3% H_2/balance Ar while the percent weight loss and heat flow were monitored.

Reaction of the samples with methane as a model hydrocarbon fuel was performed using a Micromeritics Autochem 2950 HP analyzer. The sample was heated to 500 °C in air then cycled twice between methane for 35 minutes, a helium purge for 5 minutes and air for 25 minutes. The flowing gas was analyzed using a Pfeiffer Vacuum Thermostar mass spectrometer.

BET surface areas of the perovskites were determined from N_2 adsorption at 77 K and the relative pressures (P/P_o) of 0.1–0.3 using a Quantachrome Autosorb 1-C.

Computational methods

Complementary first-principles quantum mechanical calculations were performed utilizing the Vienna Ab initio Simulation Package (VASP) code which employs spin density functional theory with a basis set constructed from plane waves.[18,19] The screened hybrid functional proposed by Heyd, Scuseria and Enzerhoff (HSE06), which mixes 25% of the exact nonlocal Fock exchange with the Perdew–Burke–Enzerhoff functional, is employed.[20] The inclusion of Hartree–Fock exchange corrects the large self-interaction error inherent in the approximate forms of exchange-correlation density functional theory and hence significantly improves the description of strongly correlated systems such as mid-to-late transition metal oxides. Core electrons were handled within the framework of the projector-augmented wave (PAW) method.[21] For Fe, La, Ba, Y, and O atoms, PAW potentials acting on eight ($4s^2$ and $3d^6$), eleven ($5s^2$, $5p^6$, $5d^1$ and $6s^2$), ten ($5s^2$, $5p^6$ and $6s^2$), eleven ($4s^2$, $4p^6$, $5s^2$ and $4d^1$) and six ($2s^2$ and $2p^4$) outer core/valence electrons, respectively.

The pseudo-wave functions were expanded in terms of plane-wave basis sets with a kinetic energy cutoff of 500 eV. The *k*-point sampling of the three-dimensional electronic Brillouin zone of the periodic tetragonal cell was performed using the Monkhorst–Pack scheme.[22] The O vacancy formation energy in $BaLaFe_2O_6$, $BaYFe_2O_6$ and $Ba_2LaFe_3O_9$ simulation cells was computed with respect to gas phase oxygen in its triplet state, according to the processes:

$$BaLaFe_2O_6 \rightarrow BaLaFe_2O_5 + 1/2O_2,$$

$$BaYFe_2O_6 \rightarrow BaYFe_2O_5 + 1/2O_2$$

and

$$Ba_2LaFe_3O_9 \rightarrow Ba_2LaFe_3O_8 + 1/2O_2$$

Monkhorst–Pack k-point mesh of $6 \times 6 \times 6$ for $BaLaFe_2O_6$, $BaYFe_2O_6$ and their reduced counterparts. For the corresponding $Ba_2LaFe_3O_9$ and $Ba_2LaFe_3O_8$, a $6 \times 6 \times 2$ mesh was utilized. Brillouin zone integration was expedited using a finite-temperature Gaussian smearing function with $\sigma = 0.05$ eV. The cell volume, cell shape and the atomic positions were allowed to relax until the total force on each atom was <0.01 eV $Å^{-1}$. In the case of the free molecule, the energy was calculated by placing it in a cubic box with dimensions of 15 Å sides and performing spin-polarized Γ-point calculations. It should be noted that the full lattice relaxations were carried out all throughout using the aforementioned hybrid functional.

Results and discussion

In this work, the oxygen storage and release properties of four perovskite materials with the general formula $A^1A^2B_2O_{5+\delta}$ were studied. The A^1 site was fixed with barium while yttrium and lanthanum were selected for the A^2 site. Yttrium and lanthanum were selected because they have been shown to be present in some of the best performing materials to date.[11–13,23] In the $Dy_{1-x}Y_xMnO_{3+\delta}$ compound, increased Y substitution was found to ease the necessary reducing conditions to convert the sample from the perovskite phase to the hexagonal phase.[24] Ease of conversion between hexagonal and orthorhombic phases has been linked to large storage capacities at low temperatures, ~400 to 425 °C.[25] Lanthanum-containing perovskite materials were also found to be excellent chemical looping candidates with a high selectivity towards CO/H_2.[4] It has also been shown that larger rare earth elements such as lanthanum help to stabilize the formation of the perovskite phase in air.[24] Additionally, the maximum oxygen content, denoted by δ, has been found to increase with increasing size of the A^2 cation.[26,27]

Iron and cobalt were selected for the B site because they are relatively light transition metals that possess multiple oxidation states which should allow for the retention of charge balance upon the removal of oxygen atoms from the lattice. Additionally, previous work with the related cobalt-containing compounds $RBaCo_4O_{7+\delta}$ and $YBaCo_{4-x}Al_xO_{7+\delta}$ demonstrated oxygen uptake/release of approximately 2700 μmol g^{-1} at temperatures as low as 400 °C.[13,14,28,29] Though previous work with cobalt has been promising, iron is a more attractive alternative because it exhibits multiple oxidation states, is environmentally benign, and is inexpensive.

The synthesis of double perovskite materials can be challenging due to their complex oxidation states and the stability of several simpler, ternary compounds. Additionally, there are several possible stacking arrangements that can lead to multiple crystal structures. Several synthetic methods, including high-temperature solid-state synthesis,[30] wet chemical routes,[31–33] and a combination of both,[11] have been previously used for the synthesis of double perovskite materials. In this work, a traditional high-temperature, solid-state synthetic method performed in air was employed as it is a well known and understood process that can allow for straightforward and simple scale-up. The reactions were performed in air because it was previously demonstrated that synthesis in air, rather than an inert or reducing environment, was more likely to result in the perovskite phase rather than the hexagonal polymorph.[24]

X-ray diffraction was used to determine the composition of the obtained samples. The $BaYCo_2O_{5+\delta}$ sample was found to crystallize into two separate perovskite crystal structures, Fig. S1.† The sample is predominantly a tetragonal perovskite structure that has been previously reported[34] but also contains a small amount of a Ba-rich cubic structure.[35] Crystallization of double perovskite compounds in two distinct perovskite crystal structures has also been reported in the related systems, $NdBaFe_2O_{5+\delta}$ and $SmBaFe_2O_{5+\delta}$.[30] In the previous study, samples with the nominal double perovskite stoichiometry were found to precipitate into two related perovskite structures at large values of δ while low values resulted in better refinements with a single structure. Additionally, a small amount of Y_2O_3 was found to be present in the $BaYCo_2O_{5+\delta}$ sample. The presence of these impurity phases is due to one of the two perovskite phases deviating slightly from the ideal 1 : 1 Ba : RE ratio of the starting mixture. This is compounded by the fact that synthesis in air does not allow for exact control of the oxygen levels. The $BaLaCo_2O_{5+\delta}$ sample was found to consist primarily of a cubic perovskite phase, Fig. S2.† There is also evidence of an orthorhombic, La-rich phase that is related to $La_4Co_3O_9$,[36] which has characteristics of both perovskite and Ruddlesden–Popper structures.

Unlike the two cobalt-containing perovskite samples, the $BaYFe_2O_{5+\delta}$ sample consisted of a single tetragonal perovskite phase, Fig. S3.† This compound is essentially isostructural with the primary phase present in the $BaYCo_2O_{5+\delta}$ sample[34] which was previously used to refine the structure of the related compound $BaYCo_{2-x}Cu_xO_5$.[37] Refinement of the powder data for this sample also identified the presence of small amounts of two ternary impurities, 0.7% $BaFe_2O_4$ (ref. 38) and 8.2% $YFeO_3$.[39] The amounts of these secondary phases as determined by Rietveld analysis, were comparable to the amounts of impurity phases in some of the samples that were studied and reported on in the related $BaYMn_2O_{5+\delta}$ system.[11] Like the $BaYCo_2O_{5+\delta}$ sample, $BaLaFe_2O_{5+\delta}$ was found to consist of two distinct perovskite phases, a tetragonal double perovskite $BaLaFe_2O_{5+\delta}$ (ref. 34) and a cubic $Ba_2LaFe_3O_{7+\delta}$.[35] Rietveld analysis determined that the sample consisted of 56.0% $BaLaFe_2O_{5+\delta}$, 40.8% $Ba_2LaFe_3O_{7+\delta}$, 2.2% $Ba_2Fe_2O_5$,[40] and 1.0% La_2O_3, Fig. 2. Additional X-ray diffraction patterns can be found in the ESI.†

Initial TGA experiments were performed to examine the storage/release capabilities of these materials by cycling between air and nitrogen at 400 °C. As expected, all four of the double perovskite samples demonstrated rapid and reversible storage and release of oxygen similar to previous work performed with other perovskite materials, Fig. 3.[11,12,41] Of particular interest is the rapid kinetics with which the reduced materials recovered to a fully oxidized state. The regeneration of the oxidized phase occurred in as little as 1.5 minutes while oxygen release was a slightly slower process requiring

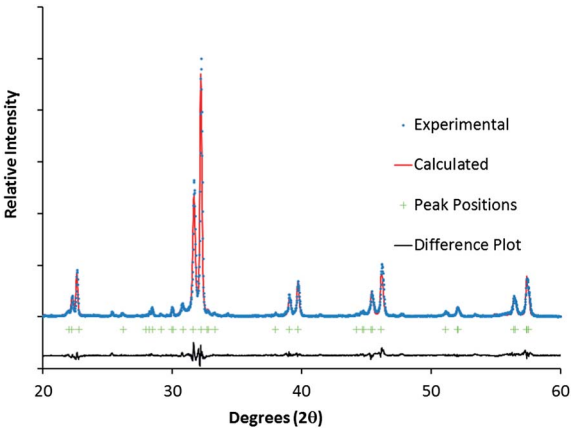

Fig. 2 Powder X-ray diffraction patterns for $BaLaFe_2O_{5+\delta}$ as a representative for the perovskite sample refinements. The experimental data are plotted in blue dots and the pattern calculated from the Rietveld refinement is plotted in red.

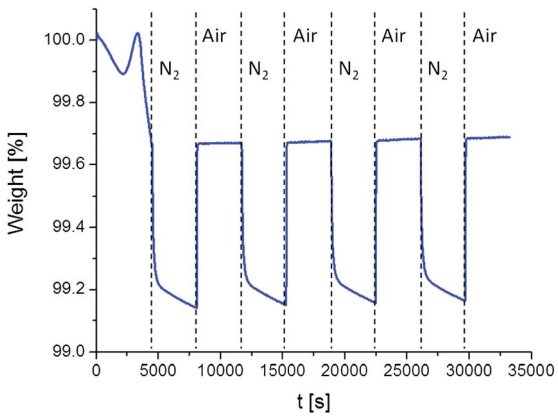

Fig. 3 Isothermal TGA curve for $BaYCo_2O_{5+\delta}$ as it is cycled between N_2 and air. The weight percent is observed to decrease sharply as the gas is changed from air to N_2 and increase sharply when the gas is changed from N_2 to air.

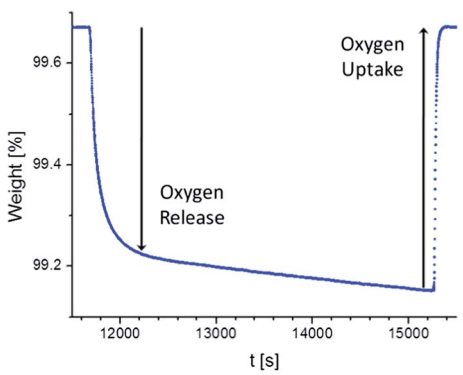

Fig. 4 Close-up view of a single oxygen release/uptake cycle. Oxygen release is rapid at first and then slows until it is mostly complete after 10 minutes. Oxygen uptake is a more rapid process requiring only 1–2 minutes to completely oxidize the material.

approximately 10 minutes, Fig. 4. The longer oxygen release times observed with TGA can be attributed to the difficulty of oxygen atoms leaving the surface of the material because the rate limiting step for oxygen release is the formation of molecules, such as water, on the particle surfaces.[11] BET measurements were performed in order to determine the effect that surface area had on oxygen capacity and kinetics of storage and release. The results for all of the samples were nearly identical, just above background, which rules out surface area significantly contributing to the observed differences between the perovskite samples.

Previous studies with perovskite materials have a demonstrated cycling capacity of up to 1875–2500 μmole of O_2 per gram of sorbent.[4,5,11] While this is a relatively large amount of oxygen, achieving these values typically requires either a reducing environment and/or relatively high temperatures. Other materials that have been studied under similar conditions to those in this work, including $Ce_{1-x}Zr_xO_{2+\delta}$ (400–500 μmole O_2 g^{-1})[42,43] and $Dy_{1-x}Y_xMnO_{3+\delta}$ (666–1200 μmole O_2 g^{-1}), have capacities comparable to the perovskite materials studied in this work.[24] In our initial low temperature work with inert environments, the amount of oxygen cycled by the perovskites varied from 25 μmole g^{-1} (0.04 wt%) for $BaYFe_2O_{5+\delta}$ to 330 μmole g^{-1} (0.53 wt%) for $BaYCo_2O_{5+\delta}$, Table 1. While these values are comparable to those of other related materials in the literature,[24] they are smaller than the best performing compounds, in particular those that had been studied in reducing environments.[11,44] In an attempt to increase the amount of cycled oxygen in these perovskite systems, TGA experiments were also conducted with cycling between air and 3% H_2 in argon.

The first set of TGA experiments with 3% H_2 were performed at 400 °C with two intended purposes: to determine if a more reducing gas mixture would result in increased mass loss in the perovskite samples and to perform initial tests with a model fuel, H_2 in this case. As in previous experiments with perovskite materials, the amount of cycled oxygen increased for all samples when nitrogen was replaced with H_2/Ar in the TGA experiments, Table 1. Unfortunately, both of the Co-containing compounds were found to decompose during the experiments, Fig. 5. The decomposition was observed as an increased mass loss with increasing cycle number in the TGA data and was evidenced in the powder X-ray diffraction data by a loss of intensity for the major double perovskite peaks. Sensitivity of Co-containing pervoskites, such as $YBaCo_2O_{5+\delta}$, to reducing environments has been reported previously.[26,45] For example, a rapid increase in resistance upon switching to 4% hydrogen in nitrogen was ascribed to the decomposition of the studied $BaLaCo_2O_{5+\delta}$ thin films.[45] Unlike their Co-containing analogs, the Fe-containing compounds were found to be stable under the more reducing atmosphere. One potential explanation for this difference is the more positive reduction potential of Co compared to Fe, 1.92 V and 0.771 V, respectively.[46]

Due to the instability of Co-containing compounds, higher temperature experiments with 3% hydrogen were only performed with $BaLaFe_2O_{5+\delta}$ and $BaYFe_2O_{5+\delta}$. Experiments were performed from 400 °C to 800 °C in 100 °C increments, Fig. 6. As

Table 1 Mass loss and corresponding number of oxygen atoms per formula unit under N_2/air and H_2/air regimes

Compound	Mass loss N_2/air (%)	Oxygen atoms lost N_2/air	Oxygen release time (min)	Oxygen storage time (min)	Mass loss H_2/air (%)	Oxygen atoms lost H_2/air
$BaYCo_2O_{5+\delta}$	0.53	0.14	8.75	1.5	2.25	0.61
$BaYFe_2O_{5+\delta}$	0.04	0.01	5.42	0.67	0.20	0.05
$BaLaFe_2O_{5+\delta}$	0.23	0.07	8.75	0.67	0.45	0.14
$BaLaCo_2O_{5+\delta}$	0.18	0.06	8.75	0.50	2.96	0.91

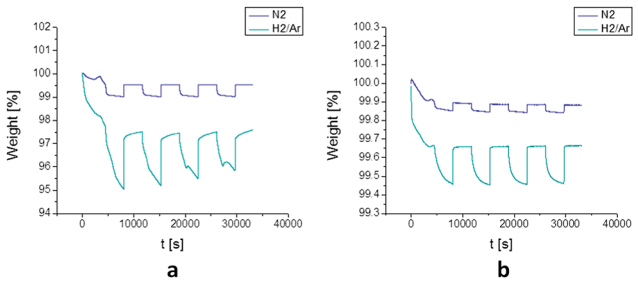

Fig. 5 A comparison of the difference in behavior between cobalt- and iron-containing samples when the reducing gas is changed from N_2 to H_2. $BaYCo_2O_{5+\delta}$ (a) can be observed to decompose as indicated in the TGA curve by a decrease in oxygen storage capacity, while the oxygen uptake and release is completely reversible for $BaYFe_2O_{5+\delta}$ (b).

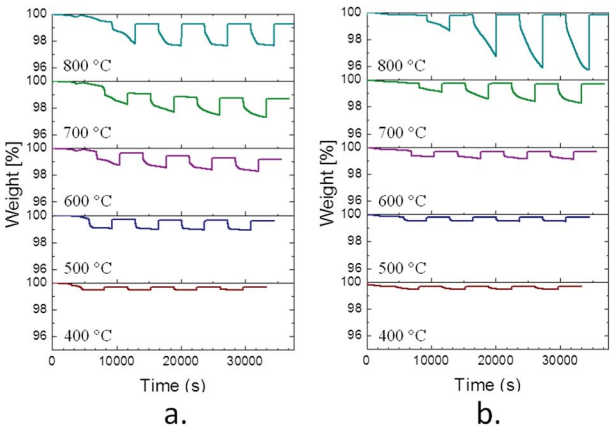

Fig. 6 Isothermal TGA curves at various temperatures for $BaLaFe_2O_{5+\delta}$ (a) and $BaYFe_2O_{5+\delta}$ (b). The oxygen capacity increases with increasing temperature for both compounds. $BaYFe_2O_{5+\delta}$ begins to decompose above 700 °C.

expected, the amount of oxygen that could be cycled increased with increasing temperature, Fig. 7. Both compounds were stable for all temperatures up to 700 °C. At 800 °C, $BaLaFe_2O_{5+\delta}$ performed well, but $BaYFe_2O_{5+\delta}$ was found to decompose, as indicated by an increasing mass loss with increasing cycle number similar to the behavior exhibited by the Co-containing materials, Fig. 5. X-ray diffraction was performed both before and after oxygen storage/release cycles and verified that at moderate temperatures the samples remained unchanged following reaction; however, at temperatures above 700 °C, $BaYFe_2O_{5+\delta}$ was decomposed into $BaFeO_3$ and $YFeO_3$. Based upon stability and rapid kinetics, the most promising sample for oxygen carrier applications is $BaLaFe_2O_{5+\delta}$.

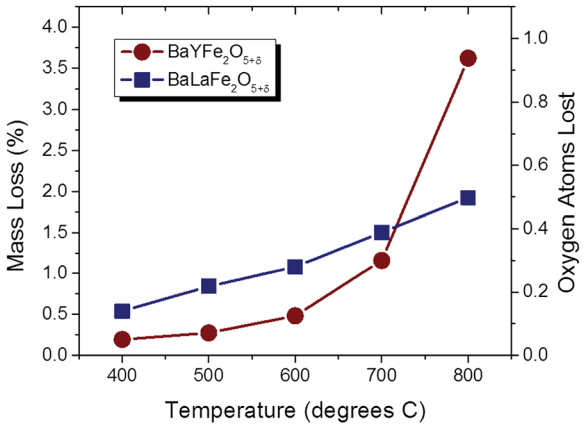

Fig. 7 Mass loss and corresponding number of oxygen atoms per formula unit for the iron-containing perovskites as a function of temperature.

First-principles DFT calculations were carried out in order to probe the origins of the differences in the oxygen storage capacities of the Fe-containing perovskites. For reference, we first calculated the bulk properties of the defect free materials. The $BaYFe_2O_{5+\delta}$ sample with $\delta = 1$, contains only a single perovskite phase. It is categorized as a stoichiometric double perovskite ($AA'B_2O_6$) possessing a modified perovskite structure (ABO_3) where the two BO_6 octahedra are arranged in two interleaving fcc sublattices. In this phase, the B sites contain Fe metal ions while the A and A′ sites are occupied by smaller Y and larger Ba atoms arranged in a layered fashion. The two FeO_6 octahedra undergo cooperative tilting distortions due to the large size of the barium atoms causing this phase to crystallize

Table 2 Calculated atomic parameters and lattice constants for $BaYFe_2O_{5+\delta}$, $BaLaFe_2O_{5+\delta}$, and $Ba_2LaFe_3O_{7+\delta}$

	$BaYFe_2O_6$	$BaLaFe_2O_6$	$Ba_2LaFe_3O_9$
Ba (x,y,z)	(0.0, 0.0, 0.0)	(0.0, 0.0, 0.0)	(0.0, 0.0, −0.002) (0.0, 0.0, 0.336)
Y (x,y,z)	(0.0, 0.0, 0.5)		
La (x,y,z)		(0.0, 0.0, 0.5)	(0.0, 0.0, 0.667)
Fe (x,y,z)	(0.5, 0.5, 0.256)	(0.5, 0.5, 0.252)	(0.0, 0.0, 0.1667)
O (x,y,z)	(0.5, 0.5, 0.5)	(0.5, 0.5, 0.5)	(0.5, 0.5, 0.667)
	(0.5, 0.0, 0.281)	(0.5, 0.0, 0.272)	(0.5, 0.0, 0.167)
	(0.5, 0.5, 0)	(0.5, 0.5, 0)	(0.5, 0.5, −0.009)
a (Å)	3.916	3.953	3.939
b (Å)	3.916	3.953	3.939
c (Å)	7.689	7.787	11.859

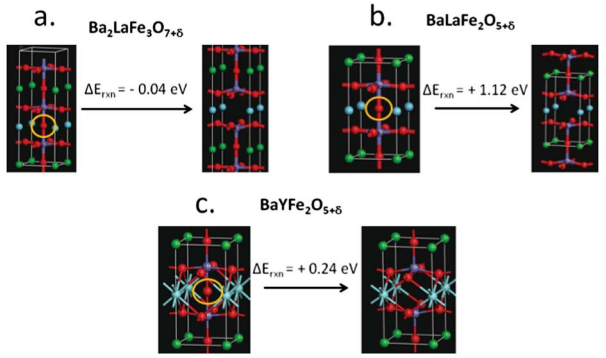

Fig. 8 Computational analysis of perovskite oxides (a) $Ba_2LaFe_3O_{7+\delta}$, (b) $BaLaFe_2O_{5+\delta}$, and (c) $BaYFe_2$ $O_{5+\delta}$. The oxygen-rich and oxygen poor structures for each compound are shown as well as the energy associated with removal of an oxygen atom.

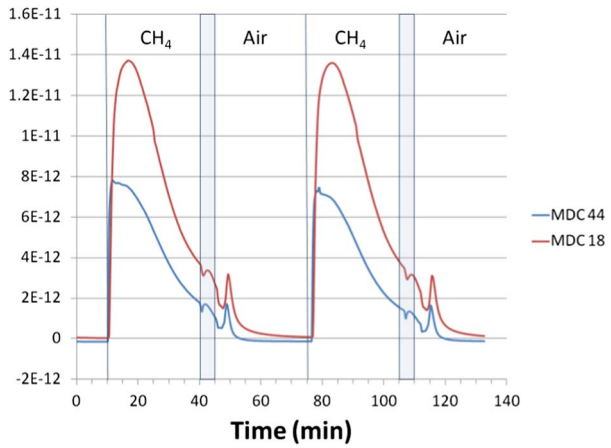

Fig. 9 CO_2 (m/z = 44) and H_2O (m/z = 18) profiles obtained from model reactions between CH_4 and $BaLaFe_2O_{5+\delta}$.

in a tetragonal structure within the *P4/nmm* space group. Our structural model for this material consists of 10 atoms (2 Fe, 6 O, 1 Ba and 1 Y) that corresponds to 1 × 1 × 2 supercell of the ideal cubic simple ABO_3 perovskite. The $BaLaFe_2O_{5+\delta}$. materials, on the other hand, contain two distinct phases: $BaLaFe_2O_{5+\delta}$. with $\delta = 1$ and $Ba_2LaFe_3O_{7+\delta}$ with $\delta = 2$. The model used for $BaLaFe_2O_6$ is similar to that of $BaYFe_2O_6$ with Y replaced by La ions. In the case of $Ba_2LaFe_3O_9$, an ordered triple perovskite model is constructed corresponding to 1 × 1 × 3 supercell of the ideal cubic simple ABO_3 perovskite. This 15-atom supercell contains layered arrangement of Ba and La (with 2 : 1 ratio) at the A-site. The calculated bulk properties are summarized in Table 2.

A first estimate of the oxygen storage capability of these materials can be obtained from the cost to form an oxygen vacancy. One neutral oxygen atom was removed from $BaYFe_2O_6$, $BaLaFe_2O_6$ and $Ba_2LaFe_3O_9$ and both the ionic position and the lattice vectors of the supercells were then relaxed. The oxygen formation energy ΔE_{rxn} is determined according to $E_{rxn} = E_{vac} + \frac{1}{2}E_{O_2} - E_{perf}$, where the three terms refer to the energy of the system with O vacancy, the gas phase O_2 molecule and the system without vacancy, respectively. The energy of O_2 in its triplet state was determined using the same level of theory. In the calculations of E_{vac} oxygen vacancy within either the Y or the La plane was considered since such configuration was found to be more energetically preferred.

DFT calculations predict that it is more energetically favorable to remove an oxygen atom from $BaYFe_2O_{5+\delta}$ than $BaLaFe_2O_{5+\delta}$, ΔE_{rxn} = +0.24 eV compared to ΔE_{rxn} = +1.12 eV, Fig. 8. If both materials consist of a single phase, this result is opposite to the experimental trend where it was observed that at a given temperature more oxygen could be cycled in $BaLaFe_2O_{5+\delta}$. As mentioned above, the $BaYFe_2O_{5+\delta}$ sample contained only a single perovskite phase while the $BaLaFe_2O_{5+\delta}$ sample contained two distinct perovskite phases. DFT calculations predicted that the energy associated with oxygen removal from the $Ba_2LaFe_3O_{7+\delta}$ perovskite phase was found to be the most energetically favorable ($\Delta E_{rxn} = -0.04$ eV), Fig. 8. As such, it is comparatively easiest to remove oxygen from $Ba_2LaFe_3O_{7+\delta}$, a result which supports the experimental findings of Fig. 7.

In order to test the viability of the Fe-containing perovskite materials for hydrocarbon combustion model reactions were performed at 500 °C with CH_4. Following methane exposure, a short helium purge was used before oxidizing the sample with air. After the sample was regenerated in air, it was used to oxidize methane for a second time to determine if the cyclic behavior observed under nitrogen and hydrogen would be reproduced when the sample was used for the combustion of a hydrocarbon fuel. The data show that CO_2 and H_2O are produced when the gas is switched from air to CH_4, which indicate that the perovskite samples are indeed capable of oxidizing a fuel, Fig. 9. To confirm that the observed results were due to the presence of the perovskite samples, a control experiment was conducted with alumina, which is known as an inert substrate in chemical looping applications. As expected, the amount of CO_2 observed in the data from the alumina run was negligible, Table 3. Therefore, the combustion of CH_4 is due to the oxygen released from the perovskite samples, making them promising oxygen carriers for chemical looping.

Not only were the samples capable of oxidizing methane, but the amount of gas production indicates that the amount of

Table 3 Amount of CO_2 produced by the iron-containing perovskites and alumina during model oxidation reactions with CH_4

Sample	Amount (g)	CO_2 produced 1st cycle (cc)	CO_2 produced 2nd cycle (cc)	CO_2 produced 1st cycle (cc g^{-1})	CO_2 produced 2nd cycle (cc g^{-1})
$BaLaFe_2O_{5+\delta}$	0.25	6.29	5.75	24.7	22.6
$BaYFe_2O_{5+\delta}$	0.26	4.48	3.5	17.2	13.5
Al_2O_3	0.26	0.93	0.59	3.6	2.3

oxygen cycled for $BaLaFe_2O_{5+\delta}$ increased from 1000 μmole g^{-1} as determined from the TGA experiments to1789 μmole g^{-1} determined from the amount of CO_2 produced in the model reactions. Though not directly comparable because the values are based on cycling between air and H_2, the amount of oxygen cycled by $BaLaFe_2O_{5+\delta}$ in the model reaction experiments is larger than the oxygen cycled by $Ce_{1-x}Zr_xO_{2+\delta}$ and some of the theoretical values for $Dy_{1-x}Y_xMnO_{3+\delta}$.[24,47] Based on their stability, oxygen storage capacities, rapid kinetics, and proven capability of oxidizing methane, $BaLaFe_2O_{5+\delta}$ and $BaYFe_2O_{5+\delta}$ are promising materials for a variety of oxygen storage applications.

Conclusions

A series of perovskite samples, $BaLnM_2O_{5+\delta}$ (Ln = Y, La and M = Fe, Co) was prepared and their oxygen uptake and release capabilities were studied. All of the samples tested demonstrated rapid and reversible oxygen uptake and release when cycled between nitrogen and air. When the gas was changed from nitrogen to hydrogen, the amount of oxygen that could be stored and released by iron-containing compounds increased; however, the cobalt containing samples were found to decompose. Further temperature dependent studies with iron-containing samples showed that the oxygen capacity increased with increasing temperature. Iron-containing perovskites were also demonstrated to oxidize methane in a model chemical looping reaction.

References

1 S. Shelley, *Chem. Eng. Prog.*, 2009, **105**, 6–10.
2 B. H. Sakakini, Y. H. Taufiq-Yap and K. C. Waugh, *J. Catal.*, 2000, **189**, 253–262.
3 S. Pei, M. S. Kleefisch, T. P. Kobylinski, J. Faber, C. A. Udovich, V. Zhangmccoy, B. Dabrowski, U. Balachandran, R. L. Mieville and R. B. Poeppel, *Catal. Lett.*, 1995, **30**, 201–212.
4 M. Ryden, A. Lyngfelt, T. Mattisson, D. Chen, A. Holmen and E. Bjorgum, *Int. J. Greenhouse Gas Control*, 2008, **2**, 21–36.
5 J. E. Readman, A. Olafsen, Y. Larring and R. Blom, *J. Mater. Chem.*, 2005, **15**, 1931–1937.
6 P. D. Battle, T. C. Gibb, P. Lightfoot and M. Matsuo, *J. Solid State Chem.*, 1990, **85**, 38–43.
7 X. F. Hao, Y. H. Xu, M. F. Lv, D. F. Zhou, Z. J. Wu and J. Meng, *Inorg. Chem.*, 2008, **47**, 4734–4739.
8 S. Chang, P. Karen, M. P. Hehlen, F. R. Trouw and R. J. McQueeney, *Phys. Rev. Lett.*, 2007, **99**, 037202.
9 A. K. Kundu, B. Raveau, V. Caignaert, E. L. Rautama and V. Pralong, *J. Phys.: Condens. Matter*, 2009, **21**, 056007.
10 D. J. Chen, F. C. Wang, H. G. Shi, R. Ran and Z. P. Shao, *Electrochim. Acta*, 2012, **78**, 466–474.
11 T. Motohashi, T. Ueda, Y. Masubuchi, M. Takiguchi, T. Setoyama, K. Oshima and S. Kikkawa, *Chem. Mater.*, 2010, **22**, 3192–3196.
12 H. S. Hao, L. Zheng, Y. F. Wang, S. J. Liu and X. Hu, *J. Rare Earths*, 2007, **25**, 275–281.
13 M. Karppinen, H. Yamauchi, S. Otani, T. Fujita, T. Motohashi, Y. H. Huang, M. Valkeapaa and H. Fjellvag, *Chem. Mater.*, 2006, **18**, 490–494.
14 T. Motohashi, S. Kadota, H. Fjellvag, M. Karppinen and H. Yamauchi, *Mater. Sci. Eng., B*, 2008, **148**, 196–198.
15 M. Karppinen, H. Okamoto, H. Fjellvag, T. Motohashi and H. Yamauchi, *J. Solid State Chem.*, 2004, **177**, 2122–2128.
16 F. Millange, E. Suard, V. Caignaert and B. Raveau, *Mater. Res. Bull.*, 1999, **34**, 1–9.
17 M. Gillessen, M. Lumeij, J. George, R. Stoffel, T. Motohashi, S. Kikkawa and R. Dronskowski, *Chem. Mater.*, 2012, **24**, 1910–1916.
18 G. Kresse and J. Furthmuller, *Phys. Rev. B: Condens. Matter Mater. Phys.*, 1996, **54**, 11169–11186.
19 J. Hafner, *J. Comput. Chem.*, 2008, **29**, 2044–2078.
20 J. Heyd, G. E. Scuseria and M. Ernzerhof, *J. Chem. Phys.*, 2003, **118**, 8207–8215.
21 G. Kresse and D. Joubert, *Phys. Rev. B: Condens. Matter Mater. Phys.*, 1999, **59**, 1758–1775.
22 H. J. Monkhorst and J. D. Pack, *Phys. Rev. B: Solid State*, 1976, **13**, 5188–5192.
23 H. S. Hao, J. H. Cui, C. Q. Chen, L. J. Pan, J. Hu and X. Hu, *Solid State Ionics*, 2006, **177**, 631–637.
24 S. Remsen and B. Dabrowski, *Chem. Mater.*, 2011, **23**, 3818–3827.
25 O. Chmaissem, H. Zheng, A. Huq, P. W. Stephens and J. F. Mitchell, *J. Solid State Chem.*, 2008, **181**, 664–672.
26 D. Akahoshi and Y. Ueda, *J. Solid State Chem.*, 2001, **156**, 355–363.
27 A. Maignan, C. Martin, D. Pelloquin, N. Nguyen and B. Raveau, *J. Solid State Chem.*, 1999, **142**, 247–260.
28 S. Kadota, M. Karppinen, T. Motohashi and H. Yamauchi, *Chem. Mater.*, 2008, **20**, 6378–6381.
29 S. Rasanen, T. Motohashi, H. Yamauchi and M. Karppinen, *J. Solid State Chem.*, 2010, **183**, 692–695.
30 P. Karen and P. M. Woodward, *J. Mater. Chem.*, 1999, **9**, 789–797.
31 J. Linden, P. Karen, A. Kjekshus, J. Miettinen and M. Karppinen, *J. Solid State Chem.*, 1999, **144**, 398–404.
32 J. Linden, P. Karen, A. Kjekshus, J. Miettinen, T. Pietari and M. Karppinen, *Phys. Rev. B: Condens. Matter Mater. Phys.*, 1999, **60**, 15251–15260.
33 S. Barison, M. Fabrizio, S. Fasolin, F. Montagner and C. Mortalo, *Mater. Res. Bull.*, 2010, **45**, 1171–1176.
34 W. Zhou, C. T. Lin and W. Y. Liang, *Adv. Mater.*, 1993, **5**, 735–738.
35 Y. Matsumoto and J. Hombo, *J. Solid State Chem.*, 1991, **93**, 395–402.
36 O. H. Hansteen, H. Fjellvag and B. C. Hauback, *J. Mater. Chem.*, 1998, **8**, 2089–2093.
37 L. Barbey, N. Nguyen, V. Caignaert, F. Studer and B. Raveau, *J. Solid State Chem.*, 1994, **112**, 148–156.
38 H. Mitsuda, S. Mori and C. Okazaki, *Acta Crystallogr., Sect. B: Struct. Sci.*, 1971, **27**, 1263–1269.

39 D. DuBoulay, E. N. Maslen, V. A. Streltsov and N. Ishizawa, *Acta Crystallogr., Sect. B: Struct. Sci.*, 1995, **51**, 921–929.
40 X. D. Zou, S. Hovmoller, M. Parras, J. M. Gonzalezcalbet, M. Valletregi and J. C. Grenier, *Acta Crystallogr., Sect. A: Found. Crystallogr.*, 1993, **49**, 27–35.
41 L. Rormark, K. Wiik, S. Stolen and T. Grande, *J. Mater. Chem.*, 2002, **12**, 1058–1067.
42 H. He, H. Dai and C. T. Au, *Catal. Today*, 2004, **90**, 245–254.
43 R. Di Monte, P. Fornasiero, M. Graziani and J. Kaspar, *J. Alloys Compd.*, 1998, **275**, 877–885.
44 P. Singh, M. S. Hegde and J. Gopalakrishnan, *Chem. Mater.*, 2008, **20**, 7268–7273.
45 J. Liu, M. Liu, G. Collins, C. L. Chen, X. N. Jiang, W. Q. Gong, A. J. Jacobson, J. He, J. C. Jiang and E. I. Meletis, *Chem. Mater.*, 2010, **22**, 799–802.
46 S. C. G. Milazzo and V. K. Sharma, *Tables of Standard Electrode Potentials*, Wiley, Chichester, 1978.
47 Y. Nagai, T. Yamamoto, T. Tanaka, S. Yoshida, T. Nonaka, T. Okamoto, A. Suda and M. Sugiura, *Catal. Today*, 2002, **74**, 225–234.